Detection of infiltrating fibroblasts by single-cell transcriptomics in human kidney allografts

Hemant Suryawanshi[1*], Hua Yang[2], Michelle Lubetzky[2,3], Pavel Morozov[1], Mila Lagman[2], Alicia Alonso[4], Carol Li[2], Catherine Snopkowski[2], Franco B. Mueller[2], John R. Lee[2,3], Darshana M. Dadhania[2,3], Steven P. Salvatore[5], Surya V. Seshan[5], Vijay K. Sharma[2], Manikkam Suthanthiran[2,3], Thomas Tuschl[1*], Thangamani Muthukumar[2,3*]

[1]Laboratory of RNA Molecular Biology, The Rockefeller University, New York, NY 10065

[2]Division of Nephrology and Hypertension, Department of Medicine, Weill Cornell Medical College, New York, NY 10065

[3]Department of Transplantation Medicine, New York Presbyterian Hospital-Weill Cornell Medical College, New York, NY 10065

[4]Epigenomics Core Facility, Weill Cornell Medical College, New York, NY 10065

[5]Division of Renal Pathology, Department of Pathology and Laboratory Medicine, Weill Cornell Medical College, New York, NY 10065

***Corresponding authors:**

Hemant Suryawanshi. Email: hsuryawans@rockefeller.edu

Thomas Tuschl. Email: ttuschl@rockefeller.edu

Thangamani Muthukumar. Email: mut9002@med.cornell.edu

ABSTRACT

We tested the hypothesis that single-cell RNA-sequencing (scRNA-seq) analysis of human kidney allograft biopsies will reveal distinct cell types and states and yield insights to decipher the complex heterogeneity of alloimmune rejection. We selected 3 kidney biopsies from 3 individuals for scRNA-seq and processed them fresh using an identical protocol on the 10x Chromium platform; (i) HK: native kidney biopsy from a living donor, (ii) AK1: allograft kidney with transplant glomerulopathy and tubulointerstitial fibrosis, and worsening graft function, and (iii) AK2: allograft kidney after successful treatment of active antibody-mediated rejection. We generated 7217 high-quality single cell transcriptomes. Taking advantage of the recipient-donor sex mismatches, we determined that in AK1 with fibrosis, more than half of the kidney allograft fibroblasts were—unexpectedly—recipient-derived and therefore likely migratory and graft infiltrative, whereas in the AK2 without fibrosis, practically all fibroblasts were donor-derived. Furthermore, AK1 was enriched by tubular cells that overexpressed profibrotic extracellular matrix genes. AK2, eight months after successful treatment of rejection, contained endothelial cells that expressed T-cell chemoattractant cytokines. Altogether, single cell transcriptomics yielded novel mechanistic insights for individualizing the care of transplant recipients.

INTRODUCTION

Molecular approaches complementing conventional histopathology have propelled precision transplantation medicine to the bedside [1-3]. Single-cell RNA-sequencing (scRNA-seq) has provided hitherto unavailable opportunity to study cell types and cell states at an unprecedented level of precision [4-6]. Our goal was to investigate the utility of single-cell RNA-sequencing (scRNA-seq) at an individual patient level to address important conundrums in clinical transplantation. Given the complex heterogeneity of alloimmune rejection, we tested the hypothesis that single-cell transcriptomics—by enabling molecular phenotyping of the host infiltrating cells and donor parenchymal cells—will yield novel mechanistic insights for individualizing the care of transplant recipients.

Immune rejection of the allograft remains a significant challenge despite the use of potent immunosuppressive drugs [7-9]. Rejection episodes restrict the benefits of transplantation and has a documented negative effect on long-term kidney allograft survival[10]. Treatment of rejection is constrained by the limited therapeutic armamentarium focused predominantly on the adaptive arm of the immune system and despite improvement in clinical and laboratory parameters, seldom achieves histological remission [10,11]. Also, despite anti-rejection therapy, it is possible that allograft injury persists at a molecular level and perpetuates allograft dysfunction. It is tempting to speculate that effective treatment of the lingering immune injury may improve the long-term outcome of kidney transplant recipients. This, however, requires better understanding of the complex immune interactions between the recipient genome and the genome of the organ donor.

We studied two clinico-pathological scenarios: (i) chronic persistent tissue injury and worsening allograft function and (ii) resolved acute tissue injury following successful treatment of an episode of active antibody mediated rejection. These results were compared to the single-cell transcriptomes of cells isolated from a native kidney used for living-donor kidney transplantation. We resolved 12 clusters of major cell types at the first level of gene expression analysis, a subset of which was further resolved by subclustering analysis. We identified 4 distinct fibroblast subpopulations differentially present in the biopsies and made the surprising finding that more than half of the kidney allograft fibroblasts in the biopsy with chronic persistent tissue injury were kidney-recipient rather donor-derived. We also identified tubular progenitor cells with profibrotic gene signature. Finally, the transcriptomes of endothelial cell subtypes provided additional insights into the anti-allograft response.

RESULTS

Clinical characteristics and kidney biopsy specimens

A summary of the clinical and histopathological characteristics of the healthy kidney donor and the two kidney transplant recipients is provided in Table 1. Briefly, biopsy HK was obtained from a healthy 40-year old living kidney donor. The recipient who received kidney from this healthy living donor had immediate graft function and normal serum creatinine at 12 months after transplantation with no major infections or acute rejection. Biopsy HK was done at the operating room during the back-table preparation of the native kidney prior to its implantation in the recipient.

Biopsy AK1 was obtained by ultrasound guidance from a 51-year old woman. She developed end-stage kidney disease due to lupus nephritis and received a living-donor kidney transplant. She had worsening of proteinuria after the living-donor kidney transplantation and an allograft biopsy 26 months after transplantation revealed interstitial fibrosis and tubular atrophy, microvascular inflammation, and transplant glomerulopathy. The biopsy, however, did not fulfill the Banff criteria (an international standardized criteria for reporting allograft biopsies) for antibody-mediated rejection and there was no evidence for recurrence of lupus nephritis. Circulating immunoglobulin G antibodies directed against the donor HLA prior to transplant or at any time in the post-transplant period were not detected using the highly sensitive single-antigen bead assay. We did not test for non-HLA antibodies. Before transplant, she had a negative T and B cell complement-dependent cytotoxicity cross match and a negative T cell flowcytometry crossmatch. However, she had a positive B cell flowcytometry crossmatch to her kidney donor cells (donor flow cytometry B cell crossmatch) and to her own cells (auto flow cytometry B cell crossmatch). The index biopsy that was used for scRNA-seq was done for worsening proteinuria and kidney function 16 months after the initial biopsy (Fig. S1).

Biopsy AK2 was obtained by ultrasound guidance from a 29-year old man. He had end stage kidney disease due to focal and segmental glomerulosclerosis. He developed acute elevation of serum creatinine, 76 months after a living-donor kidney transplantation and allograft biopsy revealed active antibody-mediated rejection (Banff category 2) with no chronic glomerular or tubulointerstitial changes. He was treated with our transplant center protocol comprised of methylprednisolone, plasmapheresis, intravenous immunoglobulin, and bortezomib and had resolution of graft dysfunction. The index biopsy that was used for scRNA-seq was done by the treating physician for surveillance purpose 8 months after the acute rejection episode (Fig. S1). Subject AK2 had normal graft function

(serum creatinine <2 mg/dl and albuminuria <500 mg/day) at the time of the index biopsy but had persistent circulating IgG antibodies directed against the donor HLA.

Identification of distinct cell types in healthy and allograft kidneys

We conducted iterative cell clustering analysis using Seurat V3.1, an R package for exploration of single-cell data [12]. We obtained 9762 cells; 2545 cells with >25% mitochondrial content were removed from subsequent analysis. The final single-cell gene expression matrices for the three kidney biopsies were comprised of 7217 high-quality cells and separated into 12 cell clusters by gene expression (Fig. 1A, left) with no contributions from batch processing (Fig. 1A, right). Based on differential gene expression and previously established markers of cell types or states we designated these clusters as proximal tubular cells (PT1 and PT2), tubular progenitor cells (PG), loop of Henle cells, collecting duct cells, and intercalated cells (LH.CD.IC), fibroblasts (FB), endothelial cells (EC), pericytes and vascular smooth muscle cells (PC.vSMC), T cells (TC), natural killer cells (NK), B cells and plasma cells (BC.PLASMA), macrophages and dendritic cells (MAC.DC), and monocytes (MONO) (Fig. 1B and Table S1). During subclustering analysis, we removed 113 endothelial cell and pericyte doublets as well as 26 epithelial and T cell doublet.

Sex differences between kidney recipient and donor reveal migratory graft infiltrating cells

AK1 was a female recipient of a kidney from a male donor and AK2 was a male recipient of a kidney from a female donor. We took advantage of the sex mismatch between kidney recipients and their donors and monitored the expression of male-specific Y chromosome-encoded EIF1AY and DDX3Y and female-specific XIST, involved in female X chromosome inactivation, to determine recipient or donor origin of the cells in the allograft [13]. We first separated the cell clusters by individual samples and then assigned each cluster to either female or male origin based on the expression pattern of XIST, EIF1AY, and DDX3Y genes. Overall, the frequency for capture of sex-specific transcripts was higher for female cells as XIST was more abundant in expression compared to EIF1AY and DDX3Y. HK kidney was obtained from a female kidney donor and as expected, the cell clusters expressed XIST and lacked in expression of EIF1AY and DDX3Y, indicating their female origin (Fig. 1C). The assignment of the sex of cells was further improved by including Y-chromosome autosomal-region-expressed RPS4Y1 (Fig. S2).

In accord with AK1 being a female recipient of male kidney, all graft infiltrating immune cell types TC, NK, BC.PLASMA, and MAC.DC were of female origin and matched the sex of the allograft recipient. In accord with AK2 being a male recipient of female kidney, the graft infiltrating immune cell types were of male origin matching the sex of the recipient. In contrast to the infiltrating cells, the AK1 kidney parenchymal cells were male and matched the sex of the organ donor, while AK2 kidney parenchymal cells were female but also matched the donor. Importantly, XIST RNA expression was not universal across all female parenchymal cells as exemplified by absence in PT1 and PT2 in AK2 and HK female kidneys. The absence of XIST from female PT cells is likely biological rather than due to technical issues.

Unexpectedly, the majority of the FBs identified in male kidney AK1 were of female recipient origin (like the immune cells), indicating that these FBs are migratory in nature and their presence in the allograft is by infiltration of cells from the recipient (Table S2). The AK1 kidney biopsy had a Banff chronic lesion score of 2 for interstitial fibrosis (ci score), defined by interstitial fibrosis involving 26-50% of cortical area. This finding is particularly striking considering that FBs in AK2, where the biopsy had a Banff ci score of 0, defined by interstitial fibrosis involving ≤5% of cortical area, were largely matching the donor (like the kidney parenchymal cells) and not the recipient.

Comparative analysis of fibroblast-specific gene expression in healthy and allograft kidneys

To further resolve FB subtypes, we performed FB subclustering analysis and identified FB1 to FB4 (Fig. 2A, top panel), all of which expressed the canonical fibroblast marker DCN (Figure 2B). The subtypes distinguish disease (FB1 and FB4) and healthy samples (FB2 and FB3) (Figure 2A, bottom panel). FB1 was comprised of all sex-mismatched (recipient-derived) 'migratory FBs' (Fig. S3) whereas FB4 was comprised of sex-matched (donor-derived) 'transplant-organ-originating' fibroblasts of AK1 and AK2 biopsies. FB3 and FB4 were defined by expression of GGT5 and EMILIN1, markers recently reported in healthy kidney biopsy to represent interstitial fibroblasts [14]. In addition, these FBs expressed ACTA2, indicative of myofibroblast-like characteristics [14]. FB1 and FB2 expressed the secretory factors CFD, SFRP2 and SFRP4 in addition to genes implicated in promoting cell migration such as MFAP5, S100A4 and S100A10 [15]. The infiltrating FB1 cells uniquely expressed FBN1, IFI27, WISP2 and PLA2G2A. FB4 cells uniquely expressed TNC, COL4A1, COL18A1, and TGM2, genes involved in beta-1 integrin cell surface interactions and cell adhesion to the extracellular matrix, included cellular stress

response genes JUN and FOSB frequently observed in scRNA-seq due to stress of mechanical cell dissociation [16]. The migratory FB1 expression signature was devoid of immune cell or other cell lineage markers suggesting that these cells are either not derived from hematopoietic lineage or their expression is lost in the target (donor) kidney. Absence of markers of other cell lineage also suggests these are not rare cell doublets (Fig. S4). The migratory FB1 cells were comprised predominantly of female recipient-derived FB from AKI biopsy; however, we also detected 4 male recipient-derived migratory FB in the AK2 biopsy (Fig. S3).

Tubular progenitor cell populations are increased in allograft kidneys

Reclustering analysis of the epithelial cell types PT1, PT2, PG, and LH.CD.IC yielded 6 subpopulations (Fig. 3A-B). A single proximal tubular (PT) cell cluster was defined by expression of MIOX, ANPEP, and SLC13A1 genes (Fig. 3C). The tubular progenitor (PG) cells expressing PROM1, CD24, and VIM, however, separated into a major (PG1) and a minor (PG2) population. The fibrotic AK1 biopsy contributed the most to PGs (PG1 79.3% and PG2 55%) (Fig. 3D). PGs lack brush borders, are scattered throughout proximal tubules in the normal kidney and become more numerous and participate in tubular regeneration after acute tubular injury [17,18]. We note that PGs also expressed CDH2 (N-cadherin), a known marker for epithelial-mesenchymal transition (EMT) [19]. The co-expression of proximal tubular cell marker genes in PG1 suggests a more differentiated state compared to PG2. Furthermore, PG1 and PG2 are characterized by expression of injury markers HAVCR1, LCN2, and MYC, which are absent in PT (Fig. S5).

The key histological feature of AK1 kidney was interstitial fibrosis. To examine whether PG abundance and gene expression contributed to the fibrosis, we performed matrisome (the ensemble of extracellular matrix [ECM] and ECM-associated proteins) enrichment analysis [20,21] of the PT and PG subtypes (Fig. 3E) and also compared it to those of FB cells (Fig. S6). Most of the expressed collagen genes including COL4A1, COL4A2, and COL1A1, were selectively enriched in PGs and showed no or minimal expression in PT cells. Similarly, the second category of matrisome genes ‘proteoglycans’ also showed enrichment in PGs and not in PT. In addition, secreted factors including the S100A family and cytokines such as CCL2, CXCL1, and CXCL6 were abundant in PGs. The other epithelial cells of the kidney such as LH, CD, and IC-A were identified by unique expression of marker genes UMOD, AQP2, and ATP6V0D2, respectively.

Endothelial cell types in disease biopsies show a chemoattractant cytokine signature

Further investigation of endothelial cell types revealed four distinct subtypes; peritubular capillaries (PTC1-3) and descending vasa recta (DVR), primarily based on the distinct expression for PLVAP, AQP1, and SLC14A (Fig. 4A, B and Table S3). Glomerular endothelial cells did not separate out by this analysis although some ECs co-expressed glomerular endothelial markers. All EC subclusters shared expression of canonical markers such as PECAM1 and CDH5. The PTC2 subpopulation, mostly composed of AK2 cells, was characterized by the unique expression of the structurally and functionally related cytokines CXCL9, CXCL10, and CXCL11 (Fig. 4A-C). These cytokines act as chemoattractants during inflammation through binding to the receptor CXCR3 mostly expressed by activated T cells [22]. AK1 and AK2 PTCs showed a >6-fold upregulation of the cell-surface-glycoprotein-encoding SELE gene compared to HK (SELE TPM, HK: 0.6, AK1: 2.6, AK2: 4.1). Under inflammatory conditions, endothelial cells induce expression of SELE in order to facilitate trans-endothelial passage of leukocytes through adhesion to the vascular lining [23]. The PTC3 subpopulation showed higher expression of JUN, FOS and JUNB presumably induced by mechanical stress of sample processing (Fig. S7).

Pericytes and vascular smooth muscle subtypes in the kidney

The vascular smooth muscle cell and pericyte cell types were further resolved into six subpopulations: vSMC1 to 4 and PC1 and 2 (Fig. 4D, Table S3, and Fig. S8). The pericytes were characterized by PDGFRA-negative, PDGFRB-high, and RGS5-high signature (Fig. 4E). vSMC1 and 2, were dominated by the HK biopsy, and showed abundant expression of stress-induced genes (relatively more in vSMC1 than vSMC2) such as JUNB and FOSB (Fig. 4E). Interestingly, vSMC3 and 4, contributed by AK1 and AK2 biopsies, respectively, differentiated from the healthy vSMC1 and 2 by additional expression of cardiac muscle alpha actin ACTC1—likely induced due to inflammation. vSMC3 was further characterized by induction of NNMT, considered as master metabolic regulator and contributor to secretion of cytokines and oncogenic extracellular matrix of cancer-associated fibroblasts [24]. The expression of NNMT also in PTC cells was unique to the AK1 allograft with high interstitial fibrosis. The only additional difference between vSMC3 and vSMC4 was the expression of male specific EIF1AY. A higher level of stress response genes including JUNB and FOSB separated PC1 from PC2. In addition, PC2 cells expressed THY1, S100A4, and CCL2 and exclusively originated from HK cells.

Immune cell heterogeneity in the healthy and allograft kidneys

Subclustering analysis of the immune cell populations identified TC, cytotoxic TC, NK, MONO, MAC, DC, BC, PLASMA, and MAST (mast cells) cell types (Fig. 5A-C). The transplant AK1 and AK2 samples showed higher proportions of immune cell infiltrates (52% and 66%, respectively, vs. 16% in HK of all cells) (Fig. 5D). The T cells in HK were dominated by granzyme-K- (GZMK-) producing $CD8^+$ T cells, and a small subset of interferon-stimulated-gene- (ISG-) high $CD4^+$ T cells with increased expression of ISG15, MX1, RSAD2, IFIT1, and IFIT2 (Fig. 5E). ISG-high $CD4^+$ T cells were also found in AK1 and AK2. Furthermore, AK2 showed a large subpopulation of GZMK-expressing $CD8^+$ cytotoxic T cells, and a smaller subgroup of $CD8^+$ cytotoxic T cells, defined by high expression of granzyme B (GZMB) and perforin (PRF1). We also identified a minor population of central memory T cells in AK2 characterized by expression of CCR7, SELL, and TCF7. MACs expressed MS4A4A, STAB1 and SEPP1 typically considered as gene signatures of "alternatively activated" M2 macrophages. The content of NK and MONO in AK1 (0.38% and 0.44%, respectively) compared to AK2 (9.8% and 7.8%, respectively) was remarkably reduced. Interestingly, while only one PLASMA cell was detected in AK1, they represented about 1.5% of total cells in the AK2 sample. IRF1 was ≥10-fold more abundant in MACs of AK2 (TPM 3.1) compared to AK1 (TPM 0.3) and HK (TPM 0.1). IRF1 was also upregulated in cytotoxic TCs of AK2 (TPM 3.0) compared to AK1 (TPM 1.7) and HK (TPM 1.4). Given their small number, the biological relevance of immune cell heterogeneity should be interpreted with caution.

DISCUSSION

The key findings of our single-cell transcriptome analysis include: (i) allograft kidney biopsy AK1, with ongoing tubulointerstitial fibrosis, contained more recipient-derived fibroblasts in contrast to the allograft kidney AK2 biopsy with no fibrosis and almost exclusively donor-derived FBs; (ii) allograft kidney AK1 biopsy also contained most proximal tubular progenitor cells that were enriched in the expression of ECM glycoproteins, collagens, and proteoglycans, and (iii) allograft kidney AK2 biopsy, eight months after successful treatment of antibody-mediated rejection as defined by clinical and histological criteria, contained endothelial cells expressing T cell chemoattractant cytokines. Determining the frequency of these observations is essential and will require scRNA-seq studies on larger cohorts of similar phenotype.

The discovery of migratory recipient-derived fibroblast subtypes in a human allograft kidney biopsies is prompting for the investigation of molecular cues leading into recruitment of such migratory FBs to the kidney, the answer of which may hold immense therapeutic implications. The AK1 biopsy showed chronic parenchymal injury and graft dysfunction and manifested histologically as TG and interstitial fibrosis. Recent studies in animal models have demonstrated that bone-marrow-derived FBs contribute significantly to kidney fibrosis [25]. However, there is controversy on the relative contribution of different cell types including FBs, fibrocytes, pericytes, bone marrow-derived FBs, epithelial cells, and endothelial cells to myofibroblast differentiation and extracellular matrix deposition in kidney fibrosis [26]. Our observation suggests that the migratory and tissue-invasive nature of the FBs may play a crucial role in fibrosis and complements the prior observation of mesenchymal cells of host origin in the vascular and interstitial compartments of kidney allografts undergoing chronic rejection [27]. The migratory FB1 subpopulation expressed fibronectin (FBN1), interferon alpha inducible proteins 27 (IFI27), WNT1 inducible signaling pathway protein 2 (WISP2), and Complement decay-accelerating factor (CD55) uniquely. All these genes have been implicated in cancer cell migration and metastasis [28-31]. In addition, migratory FB1 and non-migratory FB4 subpopulation identified in the AK1 biopsy were differentiated by MFAP5 and S100A4 expression in the migratory FBs. Increased MFAP5 expression in stromal cells was reported to stimulate cancer cell motility and invasion and predicted poor survival, and MFAP5 in vivo silencing reduced tumor progression [15]. Calcium-binding protein S100A4 promotes metastasis and is associated with intestinal fibroblast migration in patients with Crohn's disease [32,33]. Thus, the discovery of migratory FBs expressing unique genes associated with cell mobility and migration and may provide opportunities for targeted intervention in order to ameliorate interstitial fibrosis.

The detection of PROM1- (CD133-) positive tubular progenitor (PG) cells expressing ECM glycoproteins, collagens, and proteoglycans in AK1 biopsy with interstitial fibrosis and tubular atrophy is a novel finding. While the contribution of EMT to kidney fibrosis is a subject of considerable controversy, recent evidence suggests that partial EMT is sufficient to induce the release of fibrogenic cytokines [34]. The expression of CDH2 (N-cadherin) in PGs and not any other tubular epithelial cell type, suggests PGs undergo partial EMT. The expression of injury markers seen in PGs suggest that chronic tubular injury likely induces EMT transition leading to production of extracellular matrix proteins and contribute to kidney fibrosis.

Furthermore, although PGs express tubular cell markers, they could not be matched to a previously established tubular cell subsets. PGs express several S100 proteins, a family of calcium-binding proteins involved in cell apoptosis, migration, proliferation, differentiation, energy metabolism, and inflammation. $PROM1^{+}$ cells are known to be distributed throughout the kidney and capable of expansion and limited self-renewal [35]. Identifying partial EMT in tubular progenitor cells rekindles the role of tubular cells in perpetuating fibrosis.

In AK2 biopsy, a subpopulation of endothelial cells expressed mRNA for cytokines CXCL9, CXCL10 and CXCL11 while T cells expressed the cognate receptor CXCR3. Our finding of endothelium-derived T-cell chemoattractant cytokines provides a mechanistic basis for the presence of T cells in the AK2 biopsy. Donor endothelium-derived CXCL10 as initiator of alloresponse has been previously noted in a cardiac allograft model [36]. Such communication of endothelial cells through T cell chemoattractant, eight months after successful treatment of antibody-mediated rejection, is striking and highlights the role of donor-derived endothelium in perpetuating tissue injury in the presence of circulating antibodies directed against the donor HLA. Importantly, in this recipient, even though there was clinical and histological improvement, antibodies directed against the donor HLA persisted in the circulation.

Strength of our study, despite its limited sample number, is the rapid processing of freshly collected biopsies without cryopreservation, albeit on different days. We minimized the time for transfer of the samples from the ultrasound suite or the operating room, where the biopsies were performed, to the research laboratory for generating single-cell suspensions, and from the research laboratory to the genomics core laboratory for library preparation. We used the 10x Chromium platform (10x Genomics) with high cell-capture efficiency and permitting the use of human kidney allograft biopsies with limiting amount of tissue [6]. Earlier reports on scRNA-seq of healthy and diseased human kidney tissue, both native and allograft kidney, have included a combination of single-cell and

single-nucleus sequencing [14], fresh and frozen specimens [37], multiple platforms to capture the single cells [14,38] and analyzing the transcriptome after combining cells obtained from biopsies from tumor nephrectomies and discarded donor kidneys [39]. Another strength is the use of normal kidney tissue from a living kidney donor, instead of unaffected areas of tumor nephrectomies or kidneys rejected for transplantation.

Our study has limitations. The number of study subjects was sparse, and we analyzed only three biopsies. Our findings need to be validated in more biopsies. Extrapolating from these results is challenging because of the heterogeneity in rejection and tissue sampling depth by core needle biopsy. However, having implemented a standardized protocol for sample preparation, single-cell capture, RNA-seq, and data analysis, we believe that our results are robust and have provided rich mechanistic information. Another limitation is that not every cell type is captured by our whole cell dissociation protocol, in particular podocytes. Nevertheless, we were able to capture and analyze several nephron cell types; continued refinement of tissue processing techniques is expected to further improve the types of cells captured. Finally, there are inherent limitations to the scRNA-seq technique, for example, only a fraction of mRNAs present in cells are captured and converted to cDNA and the tissue dissociation process disrupts tissue architecture and loses relative spatial positioning information of cells.

In summary, we have demonstrated the utility of scRNA-seq in interrogating intragraft events in kidney allografts. Our analysis has revealed unique cell types and cell states in kidney allograft biopsies and confirmed our hypothesis that applying scRNA-seq furthers precision transplantation medicine approaches by providing mechanistic insights and opportunities for drug target and pathway identification at hitherto unknown and unavailable resolution. With improvement in the technology, refinement in computational approaches, and decreasing operational costs, it is possible in the future to apply single-cell transcriptomics to complement conventional histopathology, in the clinic, for the idealized care of transplant recipients.

METHODS

Tissue collection, dissociation, and single-cell preparation

At the time of needle biopsy, a core of the biopsy tissue was earmarked for single-cell preparation and was transported in phosphate-buffered saline immediately to our Gene Expression Monitoring laboratory and were immediately dissociated for single-cell capture. We developed and used an in-house protocol for single-cell preparation. In brief, the sample was placed in 400 µl of freshly prepared tissue dissociation solution comprised of 100 µl Liberase TL solution (2 mg/ml, Sigma-Aldrich), 500 µl Tyrode's solution-HEPES-based (Boston BioProducts), and 200 µl DNase I solution (1 mg/ml, Stemcell technologies) and incubated at 37ºC water bath for 15 min. The cell suspension was passed through a 40 µm Falcon™ cell strainer (ThermoFisher Scientific) into a 50 ml centrifuge tube filled with 5 ml fetal bovine serum (ThermoFisher Scientific), washed through with Dulbecco's phosphate-buffered saline (ThermoFisher Scientific), and centrifuged for 5 min at 300g. Cells were resuspended in 2% bovine serum albumin (New England BioLabs) and were transferred immediately in ice to the genomics core laboratory.

Single-cell capture, library preparation, sequencing, data processing, and generation of gene expression matrix

Single-cell suspension on ice was immediately transferred to the Weill Cornell Medicine genomics core facility. scRNA-seq libraries were prepared using the Chromium Single Cell 3' Reagent Kit V2 (10x Genomics) according to the manufacturer's instructions. The library was sequenced on Illumina HiSeq 2500 platform as follows: 26 bp (Read1) and 98 bp (Read2). The sequencing was performed to obtain 150–200 million reads (each for Read1 and Read2). The 10x raw data were processed individually for 3 kidney samples using previously described Drop-seq pipeline (Drop-seq core computational protocol V1.2, http://mccarrolllab.com/dropseq/) with the following parameters. The Read1 bases 1–16 were tagged with cell barcode 'XC' and bases 17–26 were tagged with a unique molecular identifier (UMI) 'XM'. Low-quality bases containing reads were removed and the 3'-end of Read2 was trimmed to remove poly(A) sequences of six or more bases and were aligned to human genome (hg38) reference using STAR aligner (STAR_2.5.1a), allowing no more than three mismatches. The gene expression matrix was then generated using the 'MIN_BC_READ_THRESHOLD= 2' option to retain UMIs with read evidence of two or more.

scRNA-seq data analysis

Cell clustering analysis was performed collectively for all 3 samples using Seurat V3.1, an R package for exploration of single-cell data. Briefly, only those genes that were expressed in more than three cells and cells that expressed more than 200 but less than 5000 genes were retained. Ubiquitously expressed genes such as ribosomal protein-coding (RPS and RPL) and non-coding RNA (MALAT1) genes were removed. We also removed miRNA and snoRNA genes from clustering analysis. The clustering analysis was performed in an iterative manner where in round 1 the cells with >25% mitochondrial content was identified and removed from round 2 clustering analysis. In round 2 analysis, mitochondrially coded genes (MT-) were also dropped from clustering analysis. We first generated three separate objects for AK1, AK2, and HK samples using 'CreateSeuratObject' function. Next we merged these object into one object using 'merge' fucntion. Next, we separated endothelial cells, epithelial cells, immune cells and stromal cells into their individual Seurat objects and conducted at least two rounds of analysis on each to identify and remove doublet captures. Typically, doublet capture show expression of markers of two different lineages (e.g., T cells and epithelial cells). Normalization was performed applying 'logNormalize' function of Seurat. Using function 'FindVariableFeatures' ~2000 genes were identified, followed by 'ScaleData'. Next, 'RunPCA', 'FindNeighbors', 'FindClusters', and 'RunUMAP' was used with different dimensions 1:10 and resolution of 0.5 wherever these options were needed. Reduction method "umap" was used and clusters were plotted using 'DimPlot' option. To identify differentially expressed genes by each cluster, Wilcoxon rank sum test inbuilt in the Seurat package was used with parameters 'min.pct = 0.25' and 'thresh.use = 0.25'.

Subclustering analyses of the cell groups described in this manuscript were performed using similar strategy as described above. The expression of established lineage marker genes was used to assign cell types. Once the cell types were identified, average expression was calculated for each cell type followed by normalization to 10,000 to create a TPM (transcript per million)-like value. For the 'donor/recipient origin of cells' analysis, separate Seurat objects were created for HK, AK1, and AK2 cells maintaining the original cell type identity. Using 'DotPlot' function, expression of female (XIST) and male (EIF1AY, DDX3Y)-specific genes was plotted.

For cells of the peritubular capillaries (PTC), in order to perform differential gene expression analysis by samples, we could not employ the conventional differential gene expression analysis methods such as DESeq2 or edgeR, due to the small number of samples. For this analysis, we only allowed genes that had >2 TPM expression in at least one of the samples (HK, AK1, or AK2). Next, for each gene, we calculated the largest (maximal) and second

largest TPM expression values across all three samples. Finally, only the genes with at least two-fold difference between maximal and second largest TPM were reported.

Matrisome enrichment analysis

Normalized expression profiles of PT, PG1 and PG2 were generated and used for matrisome analysis. We utilized a previously described list of matrisome genes and then subset the list for each category of matrisomes (collagen, proteoglycan, and secreted factor) from the TPM expression profiles of PT, PG1, and PG2 cell types. Log_2(TPM+1) values for top expressed genes in each of the matrisome category were represented in the heatmap.

Study approval

The clinical and research activities that we report here are consistent with the principles of the "Declaration of Istanbul on Organ Trafficking and Transplant Tourism"[40]. The research protocol was approved by the Weill Cornell Medicine Institutional Review Board (protocol number: 1404015008). The transplant recipients reported herein provided written informed consent to participate in the study and the informed consent was obtained prior to their inclusion in the study.

STATEMENT ON DATA AVAILABILITY

Further information and requests for resources should be directed to and will be fulfilled by the corresponding author, Thangamani Muthukumar (mut9002@med.cornell.edu). This study did not generate new unique reagents. The scRNA-seq data files have been deposited at NCBI's Gene Expression Omnibus under the accession number GSE151671.

REFERENCES

1 Haas, M. *et al.* The Banff 2017 Kidney Meeting Report: Revised diagnostic criteria for chronic active T cell-mediated rejection, antibody-mediated rejection, and prospects for integrative endpoints for next-generation clinical trials. *Am J Transplant* **18**, 293-307, doi:10.1111/ajt.14625 (2018).

2 Naesens, M. & Anglicheau, D. Precision Transplant Medicine: Biomarkers to the Rescue. *J Am Soc Nephrol* **29**, 24-34, doi:10.1681/ASN.2017010004 (2018).

3 Loupy, A. *et al.* The Banff 2015 Kidney Meeting Report: Current Challenges in Rejection Classification and Prospects for Adopting Molecular Pathology. *Am J Transplant* **17**, 28-41, doi:10.1111/ajt.14107 (2017).

4 Varma, E., Luo, X. & Muthukumar, T. Dissecting the human kidney allograft transcriptome: single-cell RNA sequencing. *Curr Opin Organ Transplant*, doi:10.1097/MOT.0000000000000840 (2020).

5 Malone, A. F. & Humphreys, B. D. Single-cell Transcriptomics and Solid Organ Transplantation. *Transplantation* **103**, 1776-1782, doi:10.1097/TP.0000000000002725 (2019).

6 Malone, A. F., Wu, H. & Humphreys, B. D. Bringing Renal Biopsy Interpretation Into the Molecular Age With Single-Cell RNA Sequencing. *Semin Nephrol* **38**, 31-39, doi:10.1016/j.semnephrol.2017.09.005 (2018).

7 Alkadi, M. M. *et al.* Kidney allograft failure in the steroid-free immunosuppression era: A matched case-control study. *Clin Transplant* **31**, doi:10.1111/ctr.13117 (2017).

8 Clayton, P. A., McDonald, S. P., Russ, G. R. & Chadban, S. J. Long-Term Outcomes after Acute Rejection in Kidney Transplant Recipients: An ANZDATA Analysis. *J Am Soc Nephrol*, doi:10.1681/ASN.2018111101 (2019).

9 Cole, E. H., Johnston, O., Rose, C. L. & Gill, J. S. Impact of acute rejection and new-onset diabetes on long-term transplant graft and patient survival. *Clin J Am Soc Nephrol* **3**, 814-821, doi:10.2215/CJN.04681107 (2008).

10 Hart, A. *et al.* OPTN/SRTR 2017 Annual Data Report: Kidney. *Am J Transplant* **19 Suppl 2**, 19-123, doi:10.1111/ajt.15274 (2019).

11 El Ters, M. *et al.* Kidney allograft survival after acute rejection, the value of follow-up biopsies. *Am J Transplant* **13**, 2334-2341, doi:10.1111/ajt.12370 (2013).

12 Stuart, T. *et al.* Comprehensive Integration of Single-Cell Data. *Cell* **177**, 1888-1902 e1821, doi:10.1016/j.cell.2019.05.031 (2019).

13 Suryawanshi, H. *et al.* A single-cell survey of the human first-trimester placenta and decidua. *Sci Adv* **4**, eaau4788, doi:10.1126/sciadv.aau4788 (2018).

14 Wu, H. *et al.* Single-Cell Transcriptomics of a Human Kidney Allograft Biopsy Specimen Defines a Diverse Inflammatory Response. *J Am Soc Nephrol* **29**, 2069-2080, doi:10.1681/ASN.2018020125 (2018).

15 Leung, C. S. *et al.* Calcium-dependent FAK/CREB/TNNC1 signalling mediates the effect of stromal MFAP5 on ovarian cancer metastatic potential. *Nat Commun* **5**, 5092, doi:10.1038/ncomms6092 (2014).

16 van den Brink, S. C. *et al.* Single-cell sequencing reveals dissociation-induced gene expression in tissue subpopulations. *Nat Methods* **14**, 935-936, doi:10.1038/nmeth.4437 (2017).

17 Smeets, B. *et al.* Proximal tubular cells contain a phenotypically distinct, scattered cell population involved in tubular regeneration. *J Pathol* **229**, 645-659, doi:10.1002/path.4125 (2013).

18 Lindgren, D. *et al.* Isolation and characterization of progenitor-like cells from human renal proximal tubules. *Am J Pathol* **178**, 828-837, doi:10.1016/j.ajpath.2010.10.026 (2011).

19 Wheelock, M. J., Shintani, Y., Maeda, M., Fukumoto, Y. & Johnson, K. R. Cadherin switching. *J Cell Sci* **121**, 727-735, doi:10.1242/jcs.000455 (2008).

20 Hynes, R. O. & Naba, A. Overview of the matrisome--an inventory of extracellular matrix constituents and functions. *Cold Spring Harb Perspect Biol* **4**, a004903, doi:10.1101/cshperspect.a004903 (2012).

21 Suryawanshi, H. *et al.* Cell atlas of the fetal human heart and implications for autoimmune-mediated congenital heart block. *Cardiovasc Res*, doi:10.1093/cvr/cvz257 (2019).

22 Panzer, U. *et al.* Compartment-specific expression and function of the chemokine IP-10/CXCL10 in a model of renal endothelial microvascular injury. *J Am Soc Nephrol* **17**, 454-464, doi:10.1681/ASN.2005040364 (2006).

23 Silva, M., Videira, P. A. & Sackstein, R. E-Selectin Ligands in the Human Mononuclear Phagocyte System: Implications for Infection, Inflammation, and Immunotherapy. *Front Immunol* **8**, 1878, doi:10.3389/fimmu.2017.01878 (2017).

24 Eckert, M. A. *et al.* Proteomics reveals NNMT as a master metabolic regulator of cancer-associated fibroblasts. *Nature* **569**, 723-728, doi:10.1038/s41586-019-1173-8 (2019).

25 Yan, J., Zhang, Z., Jia, L. & Wang, Y. Role of Bone Marrow-Derived Fibroblasts in Renal Fibrosis. *Front Physiol* **7**, 61, doi:10.3389/fphys.2016.00061 (2016).

26 Sun, Y. B., Qu, X., Caruana, G. & Li, J. The origin of renal fibroblasts/myofibroblasts and the signals that trigger fibrosis. *Differentiation* **92**, 102-107, doi:10.1016/j.diff.2016.05.008 (2016).

27 Grimm, P. C. *et al.* Neointimal and tubulointerstitial infiltration by recipient mesenchymal cells in chronic renal-allograft rejection. *N Engl J Med* **345**, 93-97, doi:10.1056/NEJM200107123450203 (2001).

28 Gopal, S. *et al.* Fibronectin-guided migration of carcinoma collectives. *Nat Commun* **8**, 14105, doi:10.1038/ncomms14105 (2017).

29 Dho, S. H., Lim, J. C. & Kim, L. K. Beyond the Role of CD55 as a Complement Component. *Immune Netw* **18**, e11, doi:10.4110/in.2018.18.e11 (2018).

30 Liu, Y. *et al.* The emerging role of WISP proteins in tumorigenesis and cancer therapy. *J Transl Med* **17**, 28, doi:10.1186/s12967-019-1769-7 (2019).

31 Xu, L. *et al.* ATF3 downmodulates its new targets IFI6 and IFI27 to suppress the growth and migration of tongue squamous cell carcinoma cells. *PLoS Genet* **17**, e1009283, doi:10.1371/journal.pgen.1009283 (2021).

32 Boye, K. & Maelandsmo, G. M. S100A4 and metastasis: a small actor playing many roles. *Am J Pathol* **176**, 528-535, doi:10.2353/ajpath.2010.090526 (2010).

33 Cunningham, M. F., Docherty, N. G., Burke, J. P. & O'Connell, P. R. S100A4 expression is increased in stricture fibroblasts from patients with fibrostenosing Crohn's disease and promotes intestinal fibroblast migration. *Am J Physiol Gastrointest Liver Physiol* **299**, G457-466, doi:10.1152/ajpgi.00351.2009 (2010).

34 Liu, B. C., Tang, T. T., Lv, L. L. & Lan, H. Y. Renal tubule injury: a driving force toward chronic kidney disease. *Kidney Int* **93**, 568-579, doi:10.1016/j.kint.2017.09.033 (2018).

35 Bussolati, B. *et al.* Isolation of renal progenitor cells from adult human kidney. *Am J Pathol* **166**, 545-555, doi:10.1016/S0002-9440(10)62276-6 (2005).

36 Hancock, W. W. *et al.* Donor-derived IP-10 initiates development of acute allograft rejection. *J Exp Med* **193**, 975-980, doi:10.1084/jem.193.8.975 (2001).

37 Der, E. *et al.* Tubular cell and keratinocyte single-cell transcriptomics applied to lupus nephritis reveal type I IFN and fibrosis relevant pathways. *Nat Immunol* **20**, 915-927, doi:10.1038/s41590-019-0386-1 (2019).

38 Arazi, A. *et al.* The immune cell landscape in kidneys of patients with lupus nephritis. *Nat Immunol* **20**, 902-914, doi:10.1038/s41590-019-0398-x (2019).

39 Stewart, B. J. *et al.* Spatiotemporal immune zonation of the human kidney. *Science* **365**, 1461-1466 (2019).

40 International Summit on Transplant, T. & Organ, T. The Declaration of Istanbul on Organ Trafficking and Transplant Tourism. *Clin J Am Soc Nephrol* **3**, 1227-1231, doi:10.2215/CJN.03320708 (2008).

ACKNOWLEDGEMENTS

Supported in part by awards from the National Institutes of Health (NIH MERIT Award, R37-AI051652 to M. Suthanthiran, K08-DK087824 and R03-DK105270 to T. Muthukumar, and NCATS Clinical and Translational Science Award, UL1TR000457 to Weill Cornell Medical College) and an award from the Mendez National Institute of Transplantation Foundation to M. Suthanthiran. We thank ThuTrang Du, Division Administrator, Division of Nephrology, Weill Cornell Medical College, for her help with the execution of this project. We thank A. Hurley and the Research Facilitation Office staff at Rockefeller University, supported in part by the NCATS Clinical and Translational Science Award, UL1TR001866 to the Rockefeller University from the NIH, for their regulatory and administrative assistance.

AUTHOR CONTRIBUTIONS

Designed research:	H.S., H.Y., M.S., T.M.
Conducting experiments:	H.Y., M.L., A.A., C.L., C.S., V.K.S., T.M.
Acquiring data:	H.S., H.Y., M.L., A.A., F.B.M., J.R.L., D.M.D., S.P.S., S.V.S., T.T., T.M.
Analyzing data:	H.S., M.L., P.M., S.V.S., T.M.
Providing reagents:	S.V.S., T.T., M.S.
Writing the manuscript:	H.S., T.T., M.S., T.M.

STATEMENT ON COMPETING INTERESTS

The authors declare no competing interests

FIGURE LEGENDS

Figure 1. scRNA-seq applied to kidney allografts differentiated cell types and resolved recipient and donor origin based on sex-specific gene expression

(A). Uniform manifold approximation and projection (UMAP)-based visualization of 7217 individual cells obtained from the three kidney biopsy tissues. **Left Panel:** UMAP-based visualization in which different clusters represent different cell types. PT1 and PT2, proximal tubular cells 1 and 2; PG, progenitor cells; LH.CD.IC, cluster of loop of Henle, collecting duct, and intercalated cells; FB, fibroblasts; EC, endothelial cells; PC.vSMC, cluster of pericytes and vascular smooth muscle cells; TC, T lymphocytes; NK, natural killer cells; BC.PLASMA, cluster of B lymphocytes and plasma cells; MAC.DC, cluster of macrophages and dendritic cells; and MONO, monocytes. **Right Panel:** UMAP-based visualization of the same cell clusters shown in the left panel in which the cells are colored by the samples. HK-healthy kidney biopsy tissue, AK1 and AK2-allograft kidney biopsy tissues.

(B). Dot-plot showing expression of known lineage markers. The size of the dot represents the proportion of cells within each cluster expressing the marker. The intensity of the color represents the standard score for each marker across different cell clusters.

(C). Dot-plot showing the annotation of donor/recipient origin of cells in each sample based on female (XIST) and male (EIF1AY, DDX3Y)-specific gene expression patterns. HK is a female donor kidney; AK1 is a female recipient of a kidney from a male donor; AK2 is a male recipient of a kidney from a female donor. XIST gene produces X-inactive specific transcript (Xist) RNA, a non-coding RNA which is a major effector of the X chromosome inactivation. The Xist RNA is expressed only on the inactive chromosome and not on the active chromosome. Males (XY), who have only one X chromosome that is active, do not express it. Females (XX), who have one active and one inactive X chromosome, express it. In HK biopsy (female kidney), all the cells in the kidney express XIST and none express the Y chromosome markers. In AK1 biopsy (male donor and female recipient), all the kidney parenchymal cells express Y chromosome markers whereas all the recipient-derived immune infiltrating cells express XIST. In AK2 biopsy (female donor and male recipient), all the kidney parenchymal cells express XIST whereas all the recipient-derived immune infiltrating cells express the Y chromosome markers.

Figure 2. Sub-clustering of fibroblasts revealed four distinct subtypes

(A). UMAP-based visualization of subpopulations of fibroblasts. In the top panel the fibroblasts are colored by different sub-populations. In the bottom panel the cells are colored by the biopsies HK, AK1 and AK2.

(B). Violin plots depict the expression of the lineage gene markers.

Figure 3. Epithelial cell sub-clustering revealed collagen-producing tubular progenitor cells

(A). UMAP-based visualization of epithelial cells colored by different cell types. PT, proximal tubular cells; IC-A, intercalated cells type A; CD, collecting duct cells; LH, loop of Henle cells; PG, progenitor cells.

(B). UMAP-based visualization of epithelial cells colored by the biopsies HK, AK1 and AK2.

(C). Violin plot showing expression of the lineage gene markers**.**

(D). Stacked bar plots show the proportion of epithelial cells in each sample. The numbers on the right is the total number of cells.

(E). Heatmap showing top expressed genes belonging to categories of matrisome groups.

Figure 4. Sub-clustering of endothelial cells, and pericytes and vascular smooth cells

(A). UMAP-based visualization of subpopulations of endothelial cells. In the left panel the endothelial cells, are colored by different sub-populations. PTC, peritubular capillaries; DVR, descending vasa recta. In the right panel the cells are colored by the biopsies HK, AK1 and AK2.

(B). Violin plots of the expression of lineage markers of endothelial cells.

(C). Heatmap shows the differentially expressed genes among the three biopsies in PTC cells (PTC1, PTC2 and PTC3 combined).

(D). UMAP-based visualization of subpopulations of pericytes and vascular smooth muscle cells. In the left panels the pericytes and vascular smooth muscle cells are colored by different sub-populations. In the right panel the cells are colored by the biopsies HK, AK1 and AK2.

(E). Violin plots of the expression of lineage gene markers of pericytes and vascular smooth muscle cells.

Figure 5. Immune cell heterogeneity in the healthy and allograft kidneys

(A). UMAP-based visualization of immune cells colored by different cell types. TC, T lymphocytes; CTC, cytotoxic T lymphocytes; NK, natural killer cells; MONO, monocytes; MAC, macrophages; DC, dendritic cells; BC, B lymphocytes; PLASMA, plasma cells.

(B). UMAP-based visualization of immune cells colored by the biopsies HK, AK1 and AK2.

(C). Dot-plot showing expression of known lineage gene markers**.**

(D). Pie chart depicting the proportion of cell types in each biopsy sample. The immune cells are labelled in red.

(E). Bar graphs showing the different types of T cells in HK, AK1, and AK2. Central memory $CD4^+$ T cells: $CCR7^+SELL^+TCF7^+$; ISG-high $CD4^+$ T cells: $CD4^+ISG15^+$; Cytotoxic $CD8^+$ T cells: $CD8A^+GZMB^+$.

Figure 1. scRNA-seq applied to kidney allografts differentiated cell types and resolved recipient and donor origin based on sex-specific gene expression

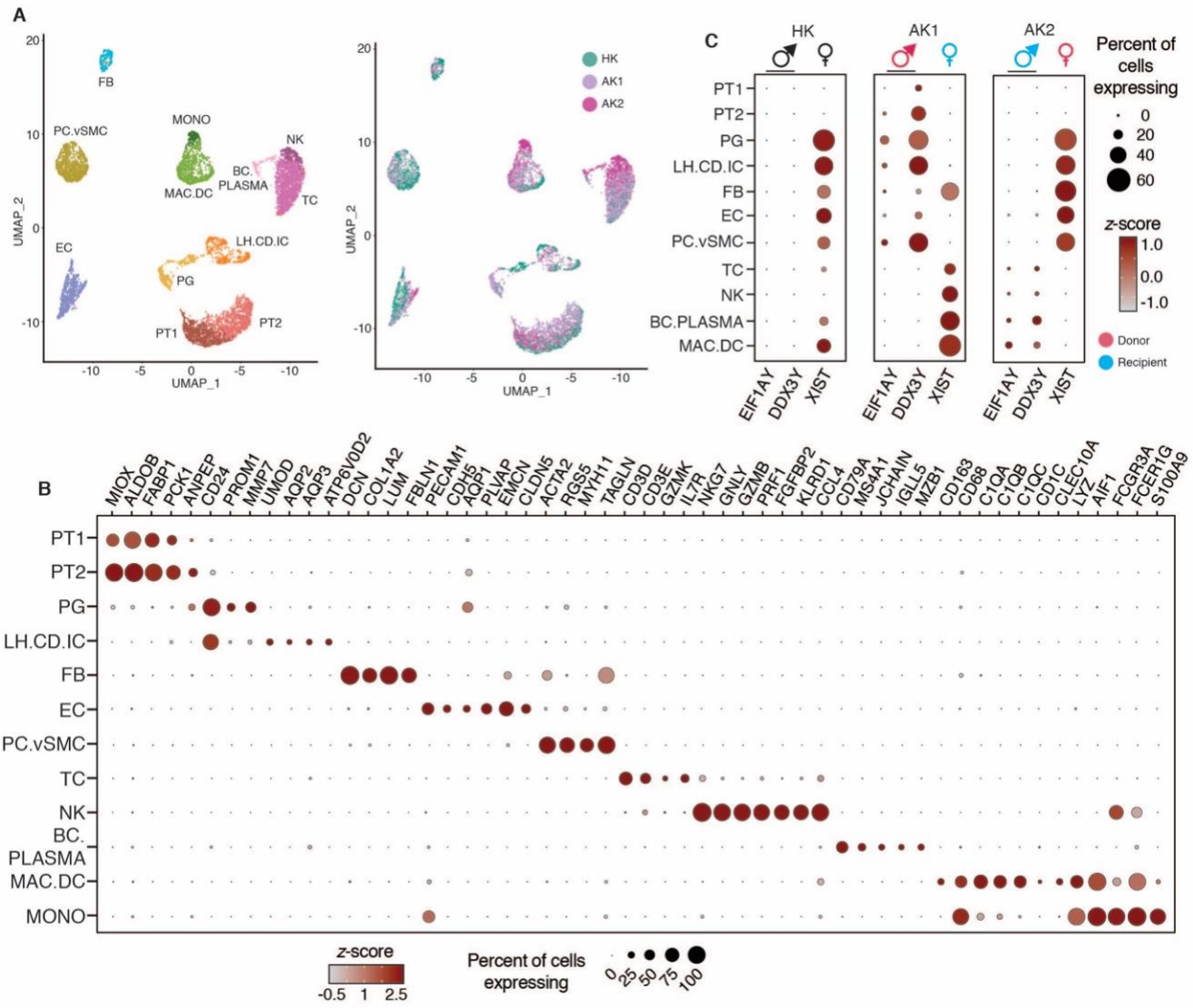

Figure 2. Sub-clustering of fibroblasts revealed four distinct subtypes

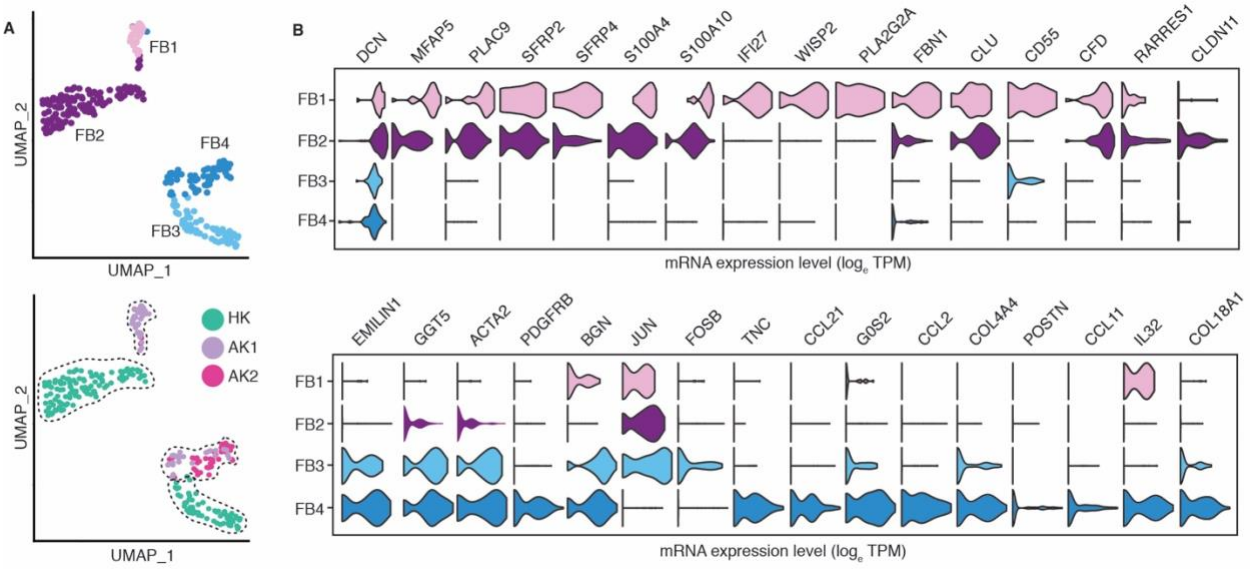

Figure 3. Epithelial cell sub-clustering revealed collagen-producing tubular progenitor cells

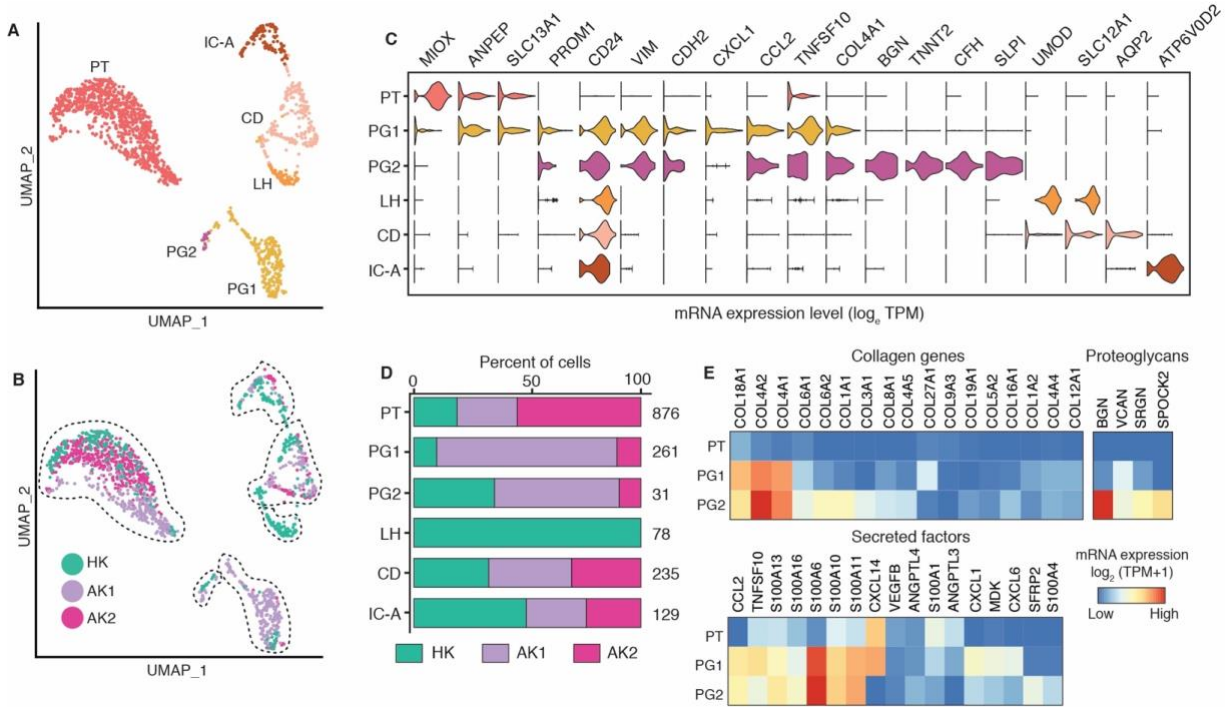

Figure 4. Sub-clustering of endothelial cells, and pericytes and vascular smooth cells

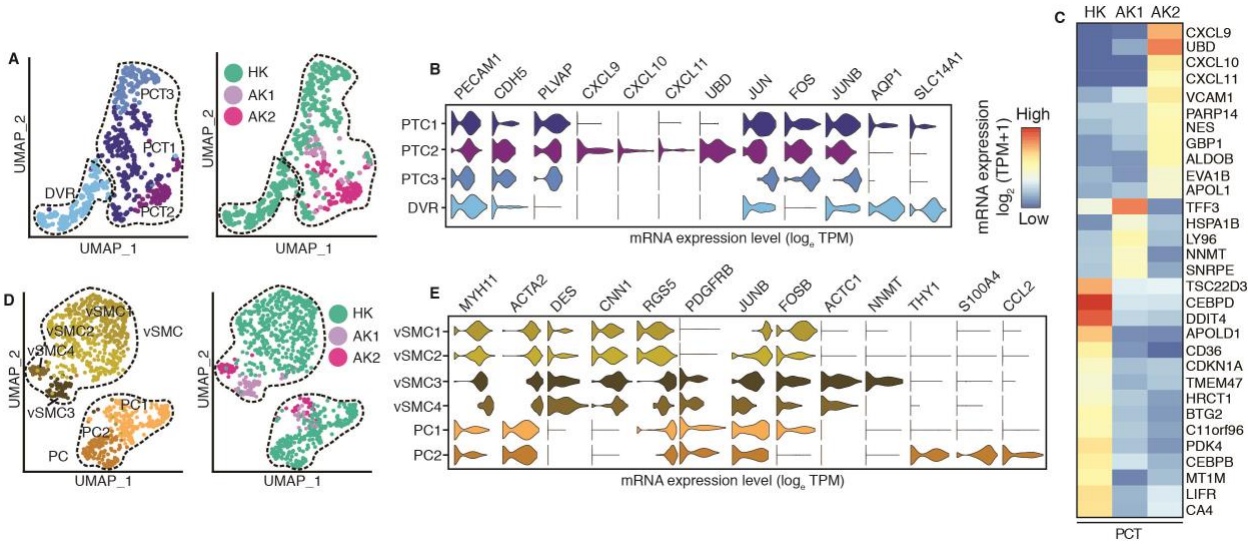

Figure 5. Immune cell heterogeneity in the healthy and allograft kidneys

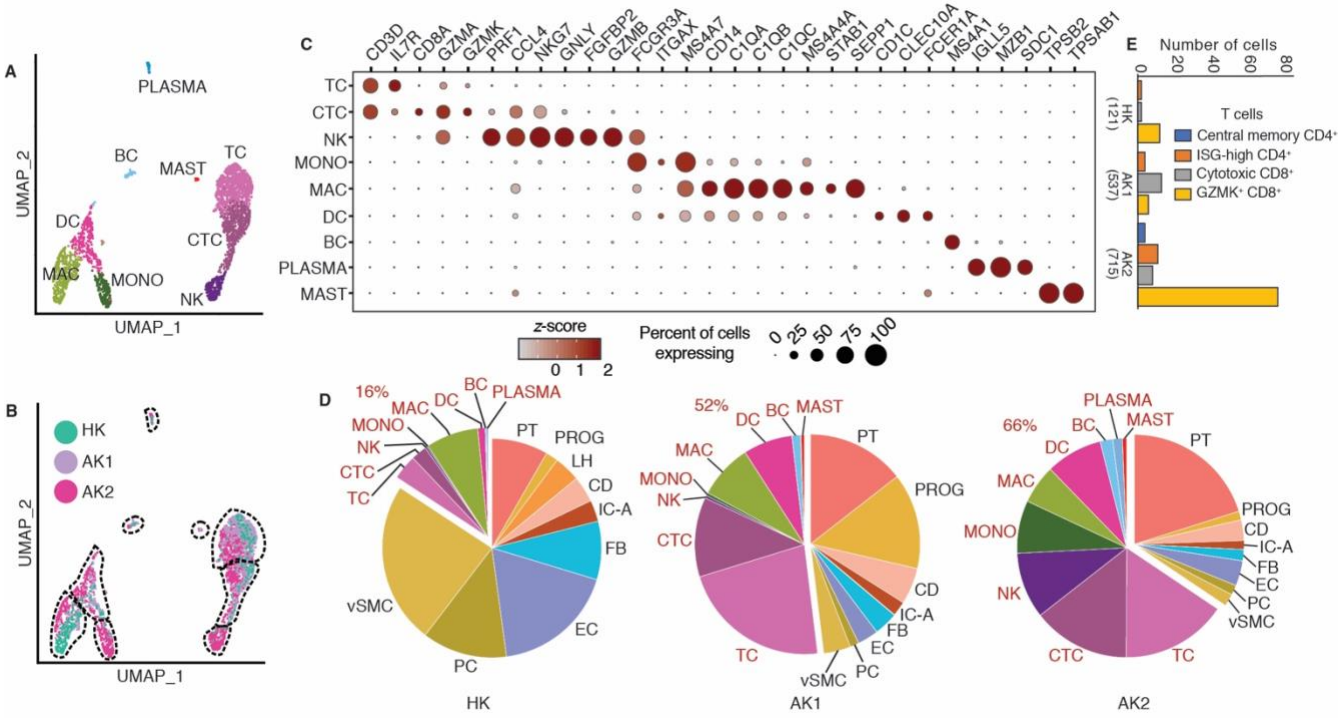

Table 1. Clinical characteristics of the three subjects whose kidney biopsies were used for scRNA-seq

Clinical Information	**Kidney Biopsies**[a]		
	Native Kidney [HK][b]	**Allograft Kidney #1** [AK1 (TG w/ graft dysfunction)][c]	**Allograft Kidney #2** [AK2 (aABMR f/u)][d]
Donor characteristics			
Living/Deceased	Living	Living	Living
Relation of the donor to recipient	Sister	Cousin	Brother
Age at donation	40 years	49 years	28 years
Gender	Female	Male	Female
Race/Ethnicity	White	Hispanic	African American
Recipient characteristics			
Age at Transplant	50	51 years	29 years
Gender	Male	Female	Male
Race/Ethnicity	White	Hispanic	African American
Native kidney disease	Diabetic nephropathy	Lupus nephritis	Focal segmental glomerulosclerosis
At the time of transplantation			
HLA-ABDR matching	1-haploidentical	1-antigen mismatch	1-haploidentical
CDC cross match[e]	Negative	Negative	Negative
Flowcytometry cross match	Not done	Donor and Auto B cell Positive[f]	Negative
Donor-specific anti-HLA antibodies[g]	Not Detected	Not Detected	Detected
Mean fluorescence intensity value	Class I - 0 Class II - 0	Class I - 0 Class II - 0	HLA Class I - 2573 against Cw5 HLA Class II MFI - 0
Induction immunosuppression	Basiliximab	Thymoglobulin	Thymoglobulin
Maintenance immunosuppression	Tacrolimus/Mycophenolate	Tacrolimus/Mycophenolate/Prednisone	Tacrolimus/Mycophenolate
From transplantation to index biopsy[h]			
Delayed graft function		No	No
BK virus/ Cytomegalovirus viremia		No	No
Number of biopsies prior to index biopsy		1	1
Time, transplant to prior biopsy		26 months	76 months
Serum creatinine at prior biopsy, mg/dl		1.11	2.16
Urine albumin:creatinine ratio at prior biopsy, mg/g		1.2	0.97
Prior biopsy findings		Severe microvascular inflammation Severe transplant glomerulopathy No tubulointerstitial fibrosis[i]	Active antibody-mediated rejection No transplant glomerulopathy No tubulointerstitial fibrosis[j]
Prior biopsy Banff lesion scores[k]		g3, ptc2, i0, t0, cg3, cptc0, ci0, ct0, C4d-	g3, ptc3, i1, t0, cg0, cptc0, ci0, ct0, C4d+
Donor-specific anti-HLA antibodies at prior biopsy		Not Detected	Detected
Mean fluorescence intensity value		Class I - 0 Class II - 0	Class I - 2760 against Cw5 Class II - 17672 against DQ4
Index biopsy used for scRNA-seq[h]			
Time, transplant to index biopsy	0 months (at donation)	42 months	84 months
Maintenance immunosuppression		Tacrolimus/Mycophenolate/ Prednisone	Tacrolimus/Mycophenolate/ Prednisone
Time, prior biopsy to index biopsy		16 months	8 months
Serum creatinine, mg/dl		2.63	1.69
Serum tacrolimus trough, ng/dl		4.6	7.8
Urine albumin:creatinine ratio, mg/g		4.8	0.22
Index biopsy findings	No inflammation No tubulointerstitial fibrosis	Severe microvascular inflammation Severe Transplant glomerulopathy Moderate tubulointerstitial fibrosis[l]	Mild microvascular inflammation No Transplant glomerulopathy No tubulointerstitial fibrosis[m]
Index biopsy Banff lesion scores[k]	g0, ptc0, i0, t0, v0, cg0, cptc0, ci0, ct0, C4d-	g3, ptc3, i1, t0, v0, cg3, cptc0, ci2, ct2, C4d-	g0, ptc1, i1, t0, v0, cg0, cptc0, ci0, ct0, C4d-
Donor-specific anti-HLA antibodies at index biopsy		Not detected	Detected
Mean fluorescence intensity value		Class I - 0 Class II - 0	Class I - 1839 against Cw5 Class II - 10512 against DQ4
From index biopsy to last follow up[h]			
Time, index biopsy to last follow up	12 months	12 months	12 months
Serum creatinine, mg/dl	1.14	Graft failure, Initiated on dialysis	1.64
Urine albumin:creatinine ratio, mg/g	21	-	0.09
Donor-specific anti-HLA antibodies	Not detected	Not detected	Detected
Mean fluorescence intensity value	Class I - 0 Class II - 0	Class I - 0 Class II - 0	Class I - 2228 against Cw5 Class II - 5361 against DQ4
Maintenance immunosuppression	Tacrolimus/Mycophenolate	None	Tacrolimus/Mycophenolate/Prednisone

[a]:Biopsies were evaluated by light, immunofluorescence and electron microscopy. Sections were stained with hematoxylin and eosin, periodic acid–Schiff, Masson trichrome, as well as for polyomavirus, immunoglobulins, complement proteins including complement factor 4 degradation product d (C4d). Each patient provided a single biopsy sample for this study. All three biopsies were done using an 18g size Bard® Monopty® disposable core biopsy instrument (Bard Biopsy, Tempe, AZ).

[b]:Native kidney biopsy tissue (HK) was obtained from the healthy kidney donor at the time of transplantation.

[c]:Allograft kidney biopsy tissue #1 (AK1) was obtained at the time of core needle biopsy of the allograft. In an earlier biopsy, chronic tissue injury and remodeling characterized by glomerular capillary basement membrane duplication (transplant glomerulopathy [TG]) was observed. Transplant glomerulopathy represents a form of chronic immune rejection likely mediated by circulating antibodies predominantly directed against the donor HLA. However, circulating IgG antibodies directed against the donor HLA prior to transplant or at any time in the post-transplant period were not detected using the highly sensitive single antigen bead assay. We did not test for non-HLA antibodies. Biopsy AK1 was done for worsening serum creatinine and proteinuria.

[d]:Allograft kidney biopsy tissue #2 (AK2) was obtained at the time of core needle biopsy of the allograft. In an earlier biopsy, active antibody-mediated rejection (aABMR), characterized histologically by inflammation of the microvasculature in the kidney and likely mediated by circulating antibodies predominantly directed against the donor HLA was observed. Kidney allograft dysfunction associated with active AMR was successfully reversed and Biopsy AK2 was done for surveillance purpose.

[e]:Complement-dependent cytotoxicity.

[f]:Flow cytometric cross match was positive for both recipient B cells (auto flow cytometry crossmatch) and kidney donor B cells (donor flow cytometry crossmatch).

[g]:Circulating immunoglobulin G antibodies in the transplant recipient directed against one or more donor HLA were measured using the highly sensitive single antigen bead assay on a Luminex platform. Mean fluorescence intensity is a measure of the degree of saturation of target antigens present on a single bead by antibodies and is used as a surrogate for the level of antibody titers. A mean fluorescence intensity value of ≥2000 is considered positive for the presence of antibodies.

[h]:The index biopsy was the kidney allograft biopsy tissue sample used for scRNA-seq.

[i]:The prior biopsy in the 51 years old female recipient had transplant glomerulopathy (chronic glomerulopathy [cg] score >0) and microvascular inflammation but did not fulfil the Banff criteria for antibody-mediated rejection.

[j]:The prior biopsy in the 29 years old male recipient was categorized as active antibody-mediated rejection, based on microvascular inflammation (MVI), positive peritubular capillary staining for complement split product 4d (C4d), and the presence of circulating antibodies directed against the donor HLA (DSA).

[k]:Biopsies were reported—based on the Banff 2017 update of the Banff '97 classification of allograft pathology[1]—independently by two transplant pathologists at our center who were blinded to the sequencing data.

[l]:The index biopsy in the 51 years old female recipient had severe transplant glomerulopathy (chronic glomerulopathy [cg] score >0) and severe microvascular inflammation but did not fulfil the Banff criteria for chronic active antibody-mediated rejection.

[m]:The index biopsy in the 29 years old male recipient had mild microvascular inflammation and did not fulfil the criteria for active antibody mediated rejection.

Supplementary Materials

SUPPLEMENTARY TABLES

Table S1. Cell type-specific gene expression

Excel File

Table S2. Cell-type specific expression of the X-Chromosome marker XIST

Cell type	HK	Cell type	AK1	Cell type	AK2
PT	0	PT	0.026925	PT	0.063701
PG	3.868948	PG	0.018473	PG	3.491369
LH	9.334275	CD	0.029711	CD	4.220906
CD	5.450415	IC.A	0	IC.A	3.703303
IC.A	4.310801	FB1	3.530406	FB4	4.782507
FB2	2.440544	FB4	0.675691	AVR	3.926241
FB3	3.04712	AVR	0.290284	vSMC	3.18347
AVR	5.393421	vSMC	0	PC	3.794725
DVR	4.014057	PC	0	TC.CTC	0
vSMC	3.586586	TC.CTC	3.808262	NK	0
PC	4.797342	MAC	4.314509	MONO	0.017436
TC.CTC	2.325882	DC	3.854761	MAC	0
MAC	5.780216	BC	9.149131	DC	0.029137
DC	3.219575			BC	0
				PLASMA	0
				MAST	0

- Cell types with greater than 10 cells are shown
- Numbers represent TPM values
- AK1: Donor - male; Recipient - female
- AK2: Donor - female; Recipient - male

Immune cells

Absolute expression values in transcript per million (TPM) of XIST gene. XIST gene produces X-inactive specific transcript (Xist) RNA, a non-coding RNA that is a major effector of the X chromosome inactivation. The Xist RNA is expressed only on the inactive chromosome and not on the active chromosome. Males (XY), who have only one X chromosome that is active, do not express it. Females (XX), who have one active and one inactive X chromosome, express it. In healthy kidney HK (female kidney), all the cells in the kidney express XIST and none express the Y chromosome markers. In AK1 biopsy (male donor and female recipient), all the kidney parenchymal cells express Y chromosome markers whereas all the recipient-derived immune infiltrating cells express XIST. In AK2 biopsy (female donor and male recipient), all the kidney parenchymal cells express XIST whereas all the recipient-derived immune infiltrating cells express the Y chromosome markers. Thus, in the three biopsies, the X and Y chromosome markers are expressed as expected. Interestingly, the fibroblasts in AK1 biopsy (male donor and female recipient), expressed XIST, proving that these were recipient-derived.

Table S3. Differential gene expression in subclustering analysis

Excel File

SUPPLEMENTARY FIGURES

Figure S1. Histopathological characteristics of kidney transplant biopsies

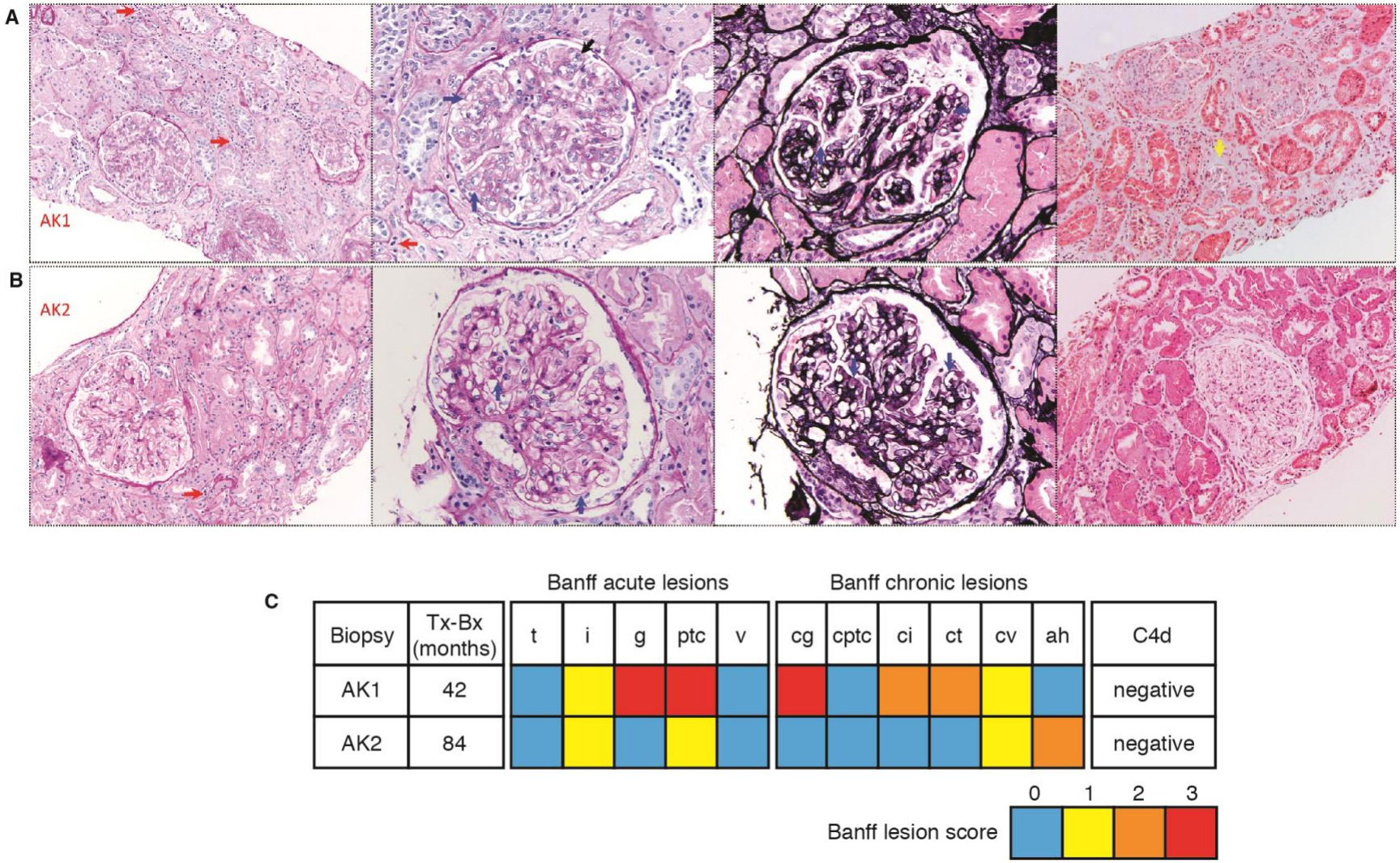

Figure depicts the histopathological characteristics of the two kidney allograft biopsies used for scRNA-Seq, AK1 and AK2. Photomicrographs show periodic acid–schiff stain at 200 (left) and 400 (center left) magnification, Jones methenamine silver stain at 400 (center right) and Masson's trichrome stain at 200 (right) magnification.

(A). Biopsy AK1 with severe transplant glomerulopathy, severe microvascular inflammation, and moderate tubulointerstitial fibrosis, was from a female patient with lupus nephritis of her native kidneys, 42 months after transplantation and 16 months after a prior biopsy that showed transplant glomerulopathy. Red arrow: peritubular capillary inflammation; Black arrow: glomerular inflammation; Blue arrow: duplication of glomerular capillary basement membrane; and Yellow arrow: interstitial fibrosis and tubular atrophy**.**

(B). Biopsy AK2 with minimal interstitial and peritubular capillary inflammation, was from a male patient with focal segmental glomerulosclerosis, 84 months after transplantation and 8 months after a prior biopsy that showed active antibody mediated rejection. Red arrow: peritubular capillary inflammation; and Blue arrow: normal glomerular capillary basement membrane.

(C). Heatmap of Banff histopathological lesion scores. Colors represent semi-quantitative Banff lesion scores from 0 to 3. Banff acute lesions include tubular inflammation (t), interstitial inflammation (i), glomerular inflammation (g), peritubular capillary inflammation (ptc), and vascular inflammation (v). Banff chronic lesions include chronic glomerulopathy (cg), peritubular capillary basement membrane multilayering (cptc), interstitial fibrosis (ci), tubular atrophy (ct)), chronic vascular lesions (cv), and arteriolar hyaline thickening (ah). Peritubular capillary staining for complement split product 4d (C4d) was negative. Biopsy HK (not shown here) was obtained from a healthy 40-year old living kidney donor and was done at the operating room during the back-table preparation of the native kidney prior to its implantation in the recipient. This biopsy had a score of zero for all acute and chronic Banff lesions.

Figure S2. UMAP-based visualization of individual cells after including the Y-chromosome gene RPS4Y1

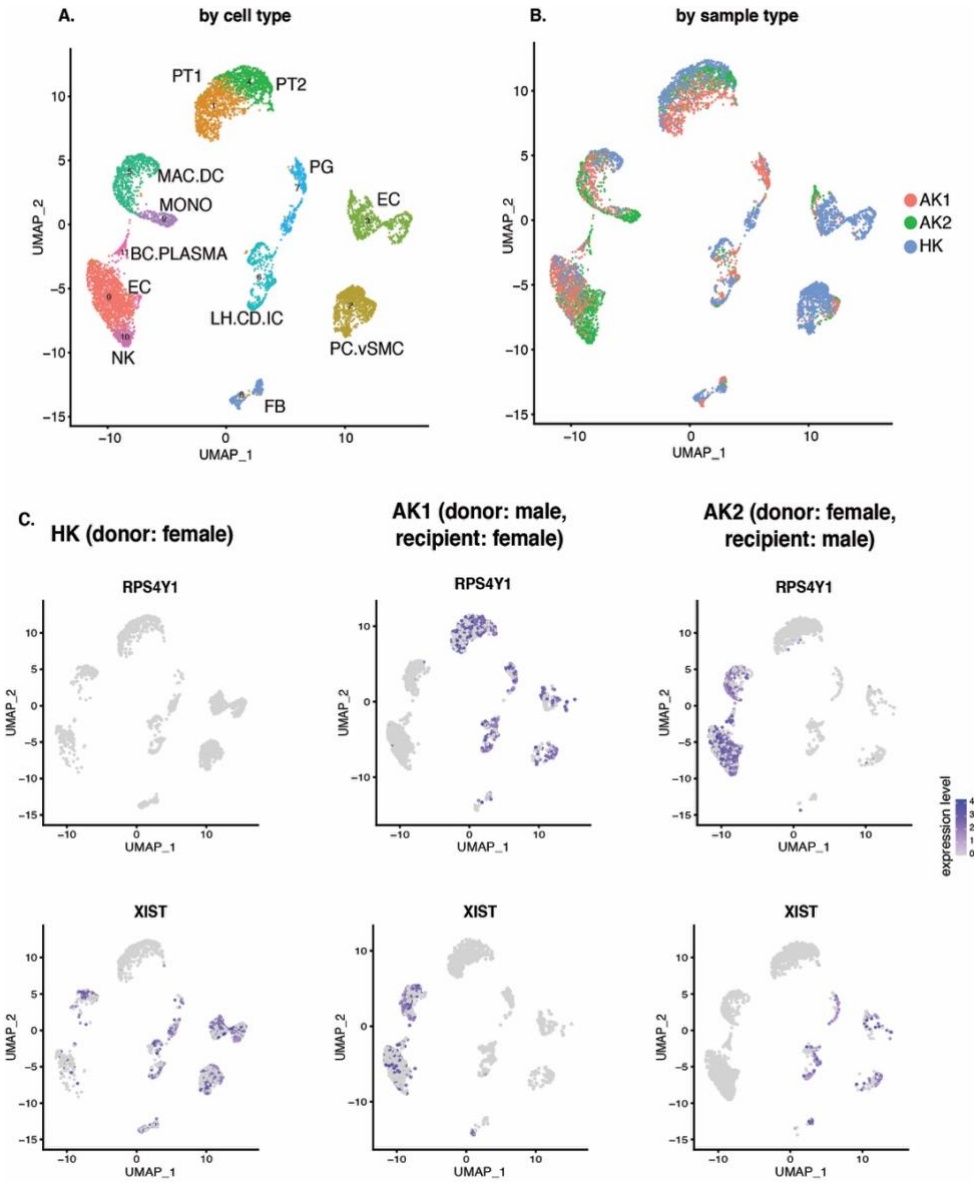

Figure depicts the UMAP-based visualization of 7217 individual cells obtained from the three kidney biopsy tissues shown in Figure 1 but including the Y-chromosome gene RPS4Y1.

(A). Uniform manifold approximation and projection (UMAP)-based visualization by cell type.

(B). UMAP-based visualization by sample type.

(C). Feature plot showing expression of the Y-chromosome gene RPS4Y1 (top panel) and X-chromosome gene XIST (bottom panel) in the three biopsies.

Figure S3. UMAP-based visualization of fibroblast subpopulation after including the Y-chromosome gene RPS4Y1

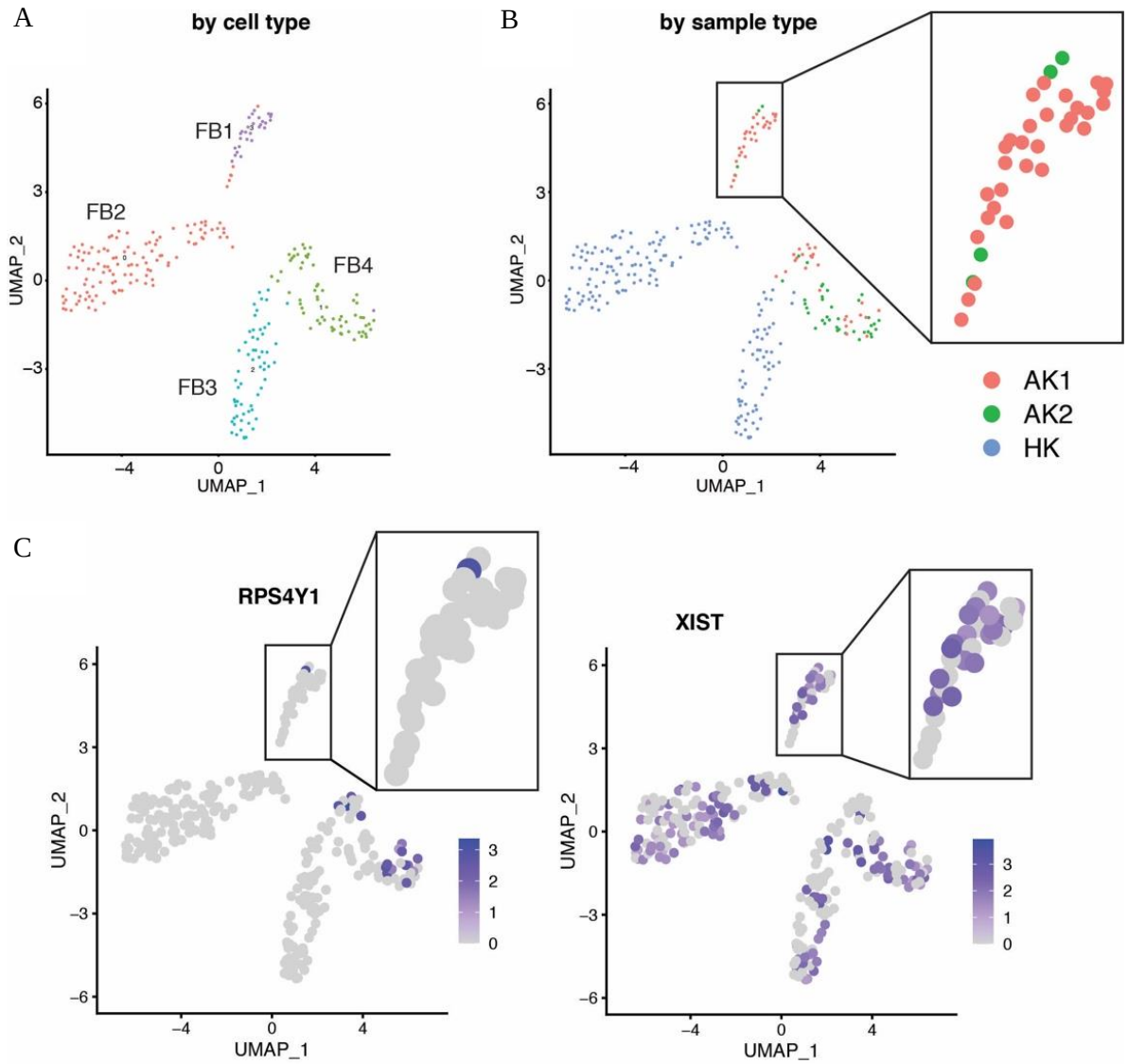

Figure depicts the UMAP-based visualization of fibroblast subpopulation obtained from the three kidney biopsy tissues shown in Figure 1 but including the Y-chromosome gene RPS4Y1.

(A). UMAP-based visualization by cell type.

(B). UMAP-based visualization by cell type. Inset depicts the enlarged view of the FB1 cell cluster.

(C). Feature plot showing expression of the Y-chromosome gene RPS4Y1 (left panel) and X-chromosome gene XIST (right panel) in the FB.

Figure S4. Expression of cell lineage markers in the fibroblast subpopulations

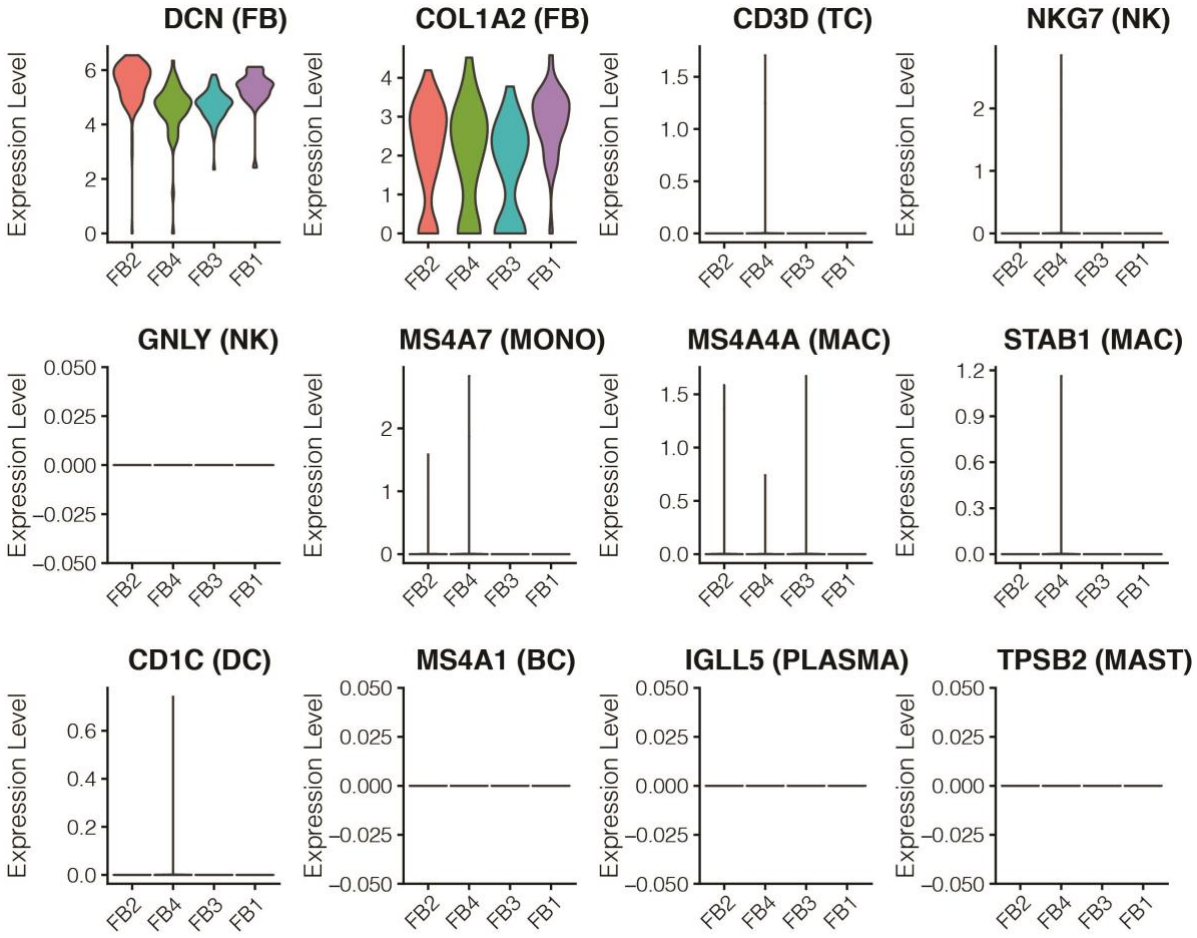

Figure depicts the violin plots showing expression of cell lineage markers in the fibroblast subpopulations. No immune cell lineage markers were expressed in the fibroblasts.

Figure S5. Analysis of kidney epithelial cell subpopulations

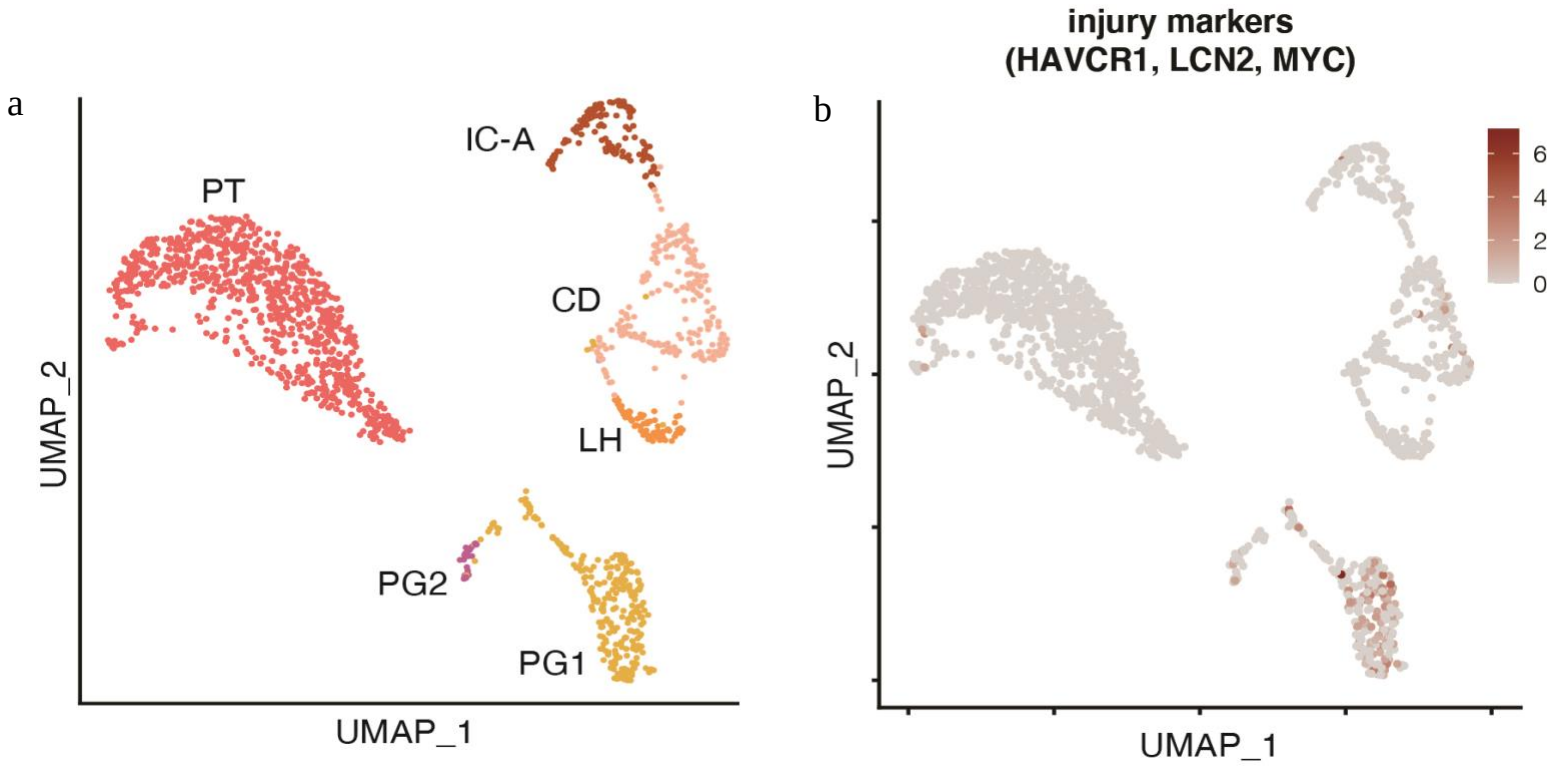

Figure depicts UMAP-based visualization of epithelial cell groups.

(A). UMAP-based visualization of epithelial cells.

(B). Feature plot showing co-expression of kidney injury markers HAVCR1, LCN2, and MYC.

Figure S6. Heatmap of top expressed genes of matrisome groups in fibroblasts, proximal tubular cells, and tubular progenitor cells

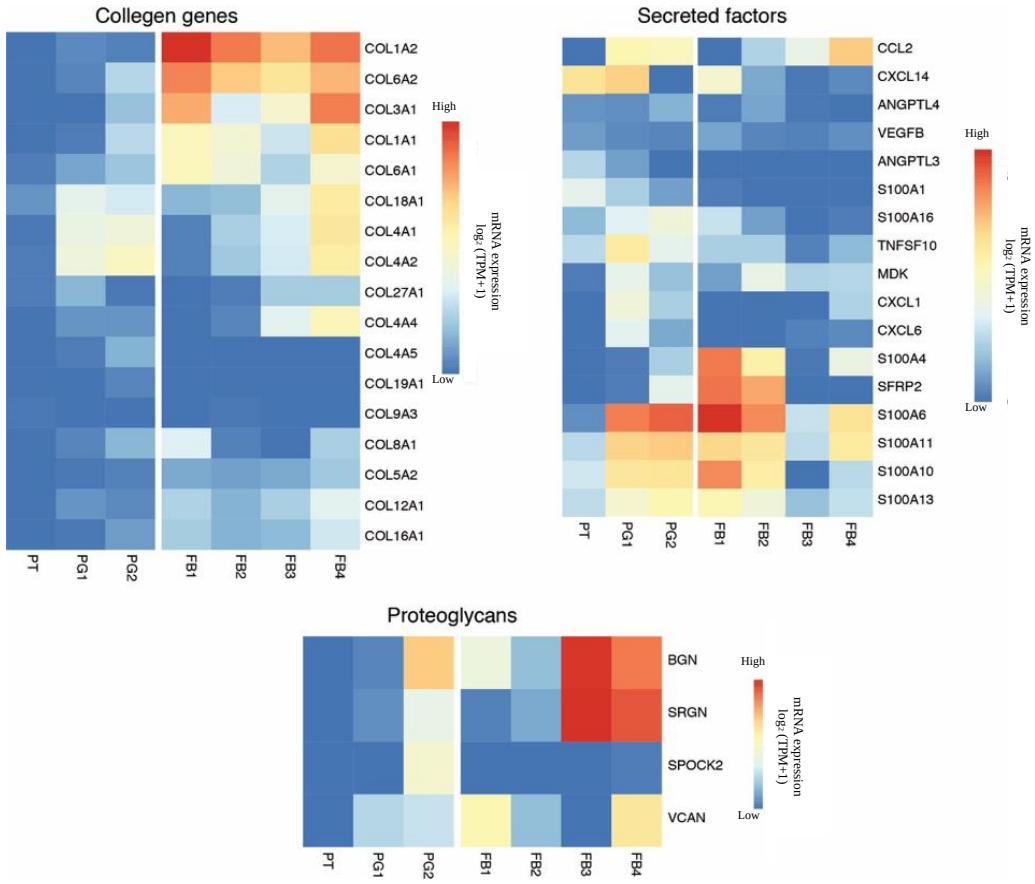

Figure depicts heatmap of the top expressed matrisome genes in the proximal tubular cells, tubular progenitor cells, and fibroblasts.

Figure S7. Differential gene expression in endothelial cell subtypes

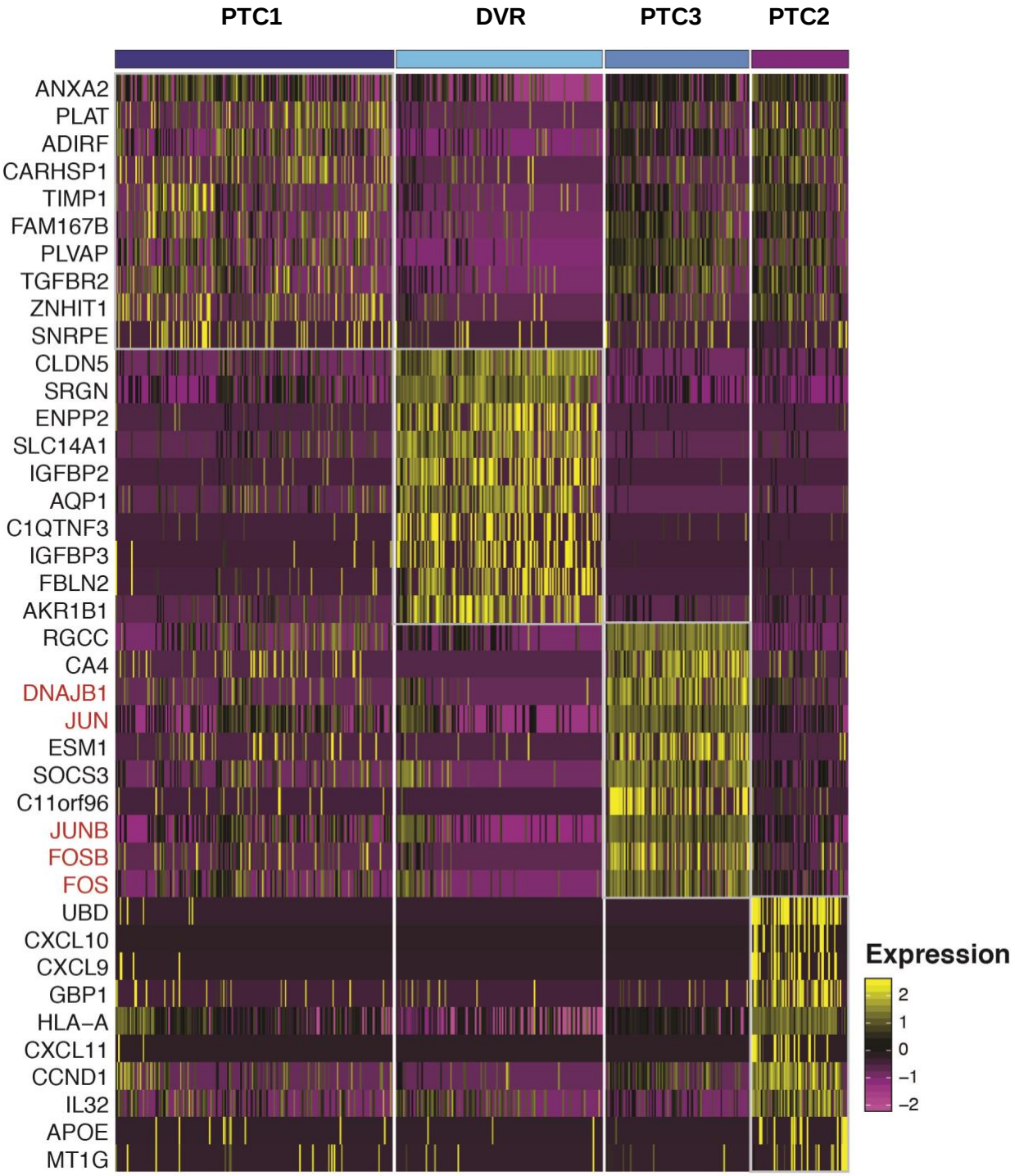

Figure depicts heatmap of the differentially expressed genes in the endothelial cell subtypes.

Figure S8. Differential gene expression in pericytes and vascular smooth muscle cells

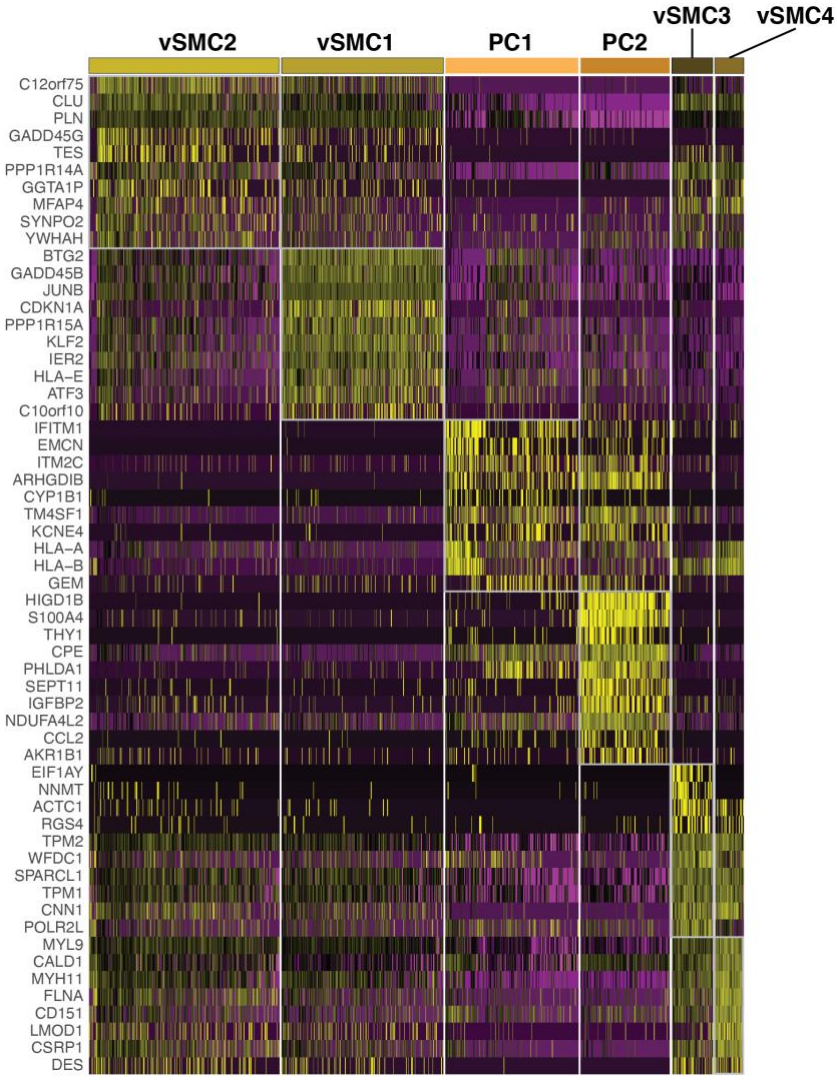

Figure depicts heatmap of differentially expressed genes in pericytes and vascular smooth muscle cells.